Development and characterisation of an AI-in-the-loop testing platform for floating wind turbines PART I: construction, validation, and benchmark testing

Xue Jiang[1], Zihao Li[1], Longbin Tao[2], Yewen Chen[3], Weiming Zeng[1], Chang Cai[3*], Guibing Zhu[1*], Qingan Li[3]

[1] Department of Naval Architecture and Marine Engineering, Zhejiang Ocean University, 1st Haidanan Road, 316000, Zhoushan, China

[2] Department of Naval Architecture, Ocean and Marine Engineering, University of Strathclyde, 100 Montrose St, Glasgow, G4 0LZ, Scotland, United Kingdom (UK)

[3]CAS Laboratory of Wind Energy Utilization, Institute of Engineering Thermophysics, Chinese Academy of Sciences, Beijing 100190, China.

***Corresponding author.** Chang Cai (caichang@iet.cn), Guibing Zhu(zhuguibing2003@163.com)

Abstract: Model testing is an inevitable means to verify design optimization because it is more economical than prototype testing and more reliable than numerical simulation. However, in the floating wind turbine experiment, the hydrodynamic Froude number and the aerodynamic Reynolds number cannot satisfy similar rules simultaneously, making the scale effect problem a major difficulty in the experiment. Therefore, this paper innovatively introduces AI-prediction-in-the-loop experimental technologies. The Froude similarity criterion is applied to model production and physical set-up. A Froude-similar wind turbine model (except for the blades) is placed in the wave flume and the floating platform moves. The response measurement data is input into the AI prediction module to perform real-time prediction of aerodynamic loads such as rotor thrust, output the calculation results and control the simulated load of the actuator, thereby realizing aerodynamic-hydrodynamic-structural coupling experiments under Froude's rules. Characterization benchmark and tank tests are carried out to validate the AI-in-the-loop testing methodology, and the results show good agreement between measured and predicted rotor thrust values across both high and low frequencies. Moreover, the time delay and systematic uncertainty of the proposed testing platform are identified for the first time.

Keywords: Wind energy, AI-in-the-loop hybrid model test, Benchmark Tests

1 Introduction

Offshore wind power has emerged as a highly promising renewable energy sector in the last decade. Its 24/7 availability and minimal environmental impact have made it an attractive option. With over 80% of wind resources located at sea in the EU [1], the offshore wind sector holds massive development potential, especially in deep-sea areas. Several initiatives aligned with the EU Green Deal have been launched to promote offshore wind power. For instance, the "RePowerEU" plan [2], released by the European Commission in March 2022, aims to achieve a cumulative installed wind power capacity of 480GW by 2030. Similarly, the UK's "energy security strategy" [3] targets an increase in offshore wind power capacity from 40GW

to 50GW by 2030. Additionally, a joint endeavour by Germany, Denmark, Belgium, and the Netherlands known as the "Esbjerg Declaration" [4] aims to develop the North Sea into a major offshore wind hub in Europe, setting a target of 65GW of installed capacity in the region by 2030. To commercialize offshore wind power, cost reduction and efficiency improvement are crucial. Model tests of Offshore Floating Wind Turbines (OFWTs) provide a cost-effective approach to optimize design schemes and explore equipment performance [5]. These tests generate more reliable results than numerical simulations while requiring less funding than full-scale sea prototypes[6]. As research on floating wind turbines is still relatively new, experimental methods are continuously being explored.

Model testing in the field of marine engineering involves simulating both gravity and inertial forces, making Froude number similarity crucial. However, the blades of a wind turbine are influenced by aerodynamic forces, which are closely related to viscosity and require Reynolds number similarity [7]. Balancing these requirements has proven challenging[8-10]. The difference in mechanical properties between the model and prototype due to Reynolds number disparities is known as the "scale effect" [11-13]. This scale effect becomes a significant challenge in model experiments for floating wind turbine systems, impacting the optimization of their design [14, 15]. Overcoming this scale effect is a critical issue in the development of efficient floating wind power systems. To address this challenge, researchers have proposed hybrid model testing methodologies as a solution[16-18]. A notable example is the real-time hybrid model experiment called ReaTHM conducted at the Norwegian University of Science and Technology[19-21]. In hybrid model experiments, actuating mechanisms are commonly used to simulate different wind load effects. For instance, a ducted fan can simulate rotor thrust, while a rotating disk with the same thrust coefficient has been used to simulate gyroscope effects. These methods have been applied in model tests of semi-submersible floating wind turbines, such as the WindFloat, at the University of California, Berkeley[22].

The authors are among the first to look at the application of machine learning technology in simulating floating wind turbine loads through an innovative interdisciplinary approach. Xue J introduced the use of deep learning methods to train neural networks using substantial simulation data from full-scale floating wind turbines[23, 24]. This resulted in the development of an intelligent machine [25, 26]capable of real-time air load prediction in fully coupled wind turbine systems. By utilizing motion response monitoring data and environmental parameters from physical models of floating platforms, the applicant successfully predicted rotor thrust. Additionally, in this paper, a prototype experimental rig with AI-prediction-in-the-loop testing methodology is constructed. Hereafter, the denomination AIReaTHM testing (AI-based Real-Time Hybrid Model testing) is used to indicate the real-time hybrid testing approach with the AI prediction machine. Moreover, a benchmark testing platform is developed to study the characteristics of the AIReaTHM testing platform. Results from the benchmark tests utilising a manoeuvrable motion simulator are used to justify its feasibility. To further investigate the performance of the newly born AI-prediction-in-the-loop testing methodology, model testing campaigns concerned with a spar-type OFWT are also carried out.

Overall, this paper is arranged in the following structure. Section 1 gives the literature review on the state-of-the-art development of the hybrid model tests of OFWTs. Section 2 introduces the novel solution of using artificial intelligence (AI) by giving a brief review of the hybrid testing methodology as well as the research objectives of this paper. Details on

constructing the AIReaTHM testing rig together with component calibrations are provided in Section 3. In Section 4, the benchmark testing method as well as the testing arrangement are demonstrated. Section 5 presents the results of the benchmark tests. In section 6, A validation of the AIReaTHM testing rig is presented by comparing the prediction values with the real-time measurement and AI prediction of the rotor thrust. Furthermore, insights into the influence of surge frequency, wind speed, turbulence, and wave spectrum on the rotor thrust are emphasised. Finally, we draw conclusions in Section 7.

2 AI-prediction-in-the-loop testing methodology

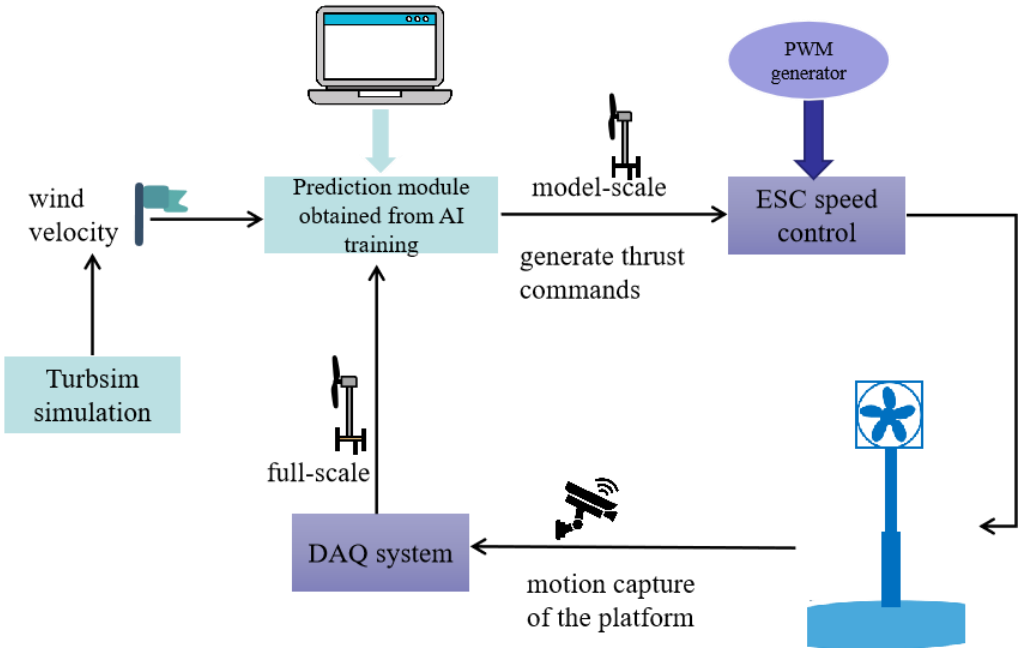

Fig. 1 Diagram of the AI-in-the-loop testing methodology

The simulation of wind loading for tank testing of OFWTs still presents a variety of severe challenges. Therefore, AI-prediction-in-the-loop hybrid approaches stand out because it allows exploring the effects of different wind environments, rotor configurations and control strategies, without complex rotor models and without generating wind field. As shown in Fig 1, Froude similarity criteria are applied in model creation and physical experiments. A Froude-similar wind turbine model (excluding blades) is placed in a wave-generating water flume. The motion response measurement data of the floating platform is input to the AI prediction module (including its acquisition and application) to predict real-time aerodynamic loads such as rotor thrust. The calculated results are outputted to control the execution mechanism to simulate the loads, thus achieving a coupled model experiment of aerodynamics, hydrodynamics, and structural dynamics under the Froude similarity rule.

To achieve the above testing methodology, a well-trained prediction model obtained by deep learning the Recurrent Neural Network (RNN) is provided, and it is designed to be deployed on a portable controller. As shown in Fig 2, the inputs to the prediction model are designed to be “surge position, surge velocity, pitch position, pitch velocity and wind velocity”, the output is rotor thrust.

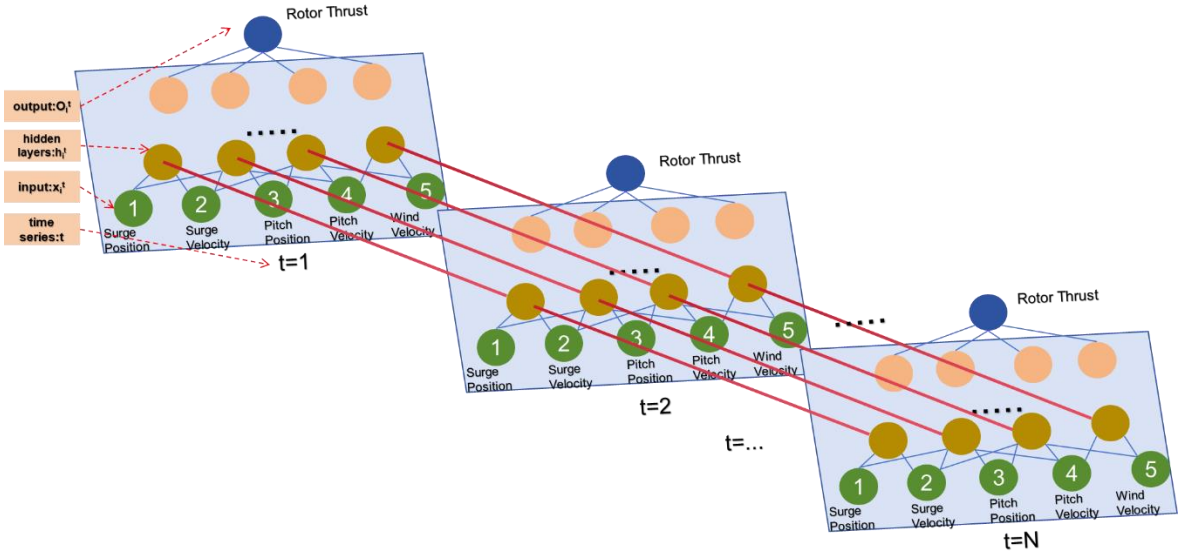

Fig. 2 Structure of the prediction model

The main purpose of using RNN in the prediction model is to obtain the potential relationship between input data and output data in the dataset. As shown in Fig 2, in addition to receiving input x (t) for each step, it will connect to the feedback information of the previous step -- the hidden state h (t-1), that is, the hidden state h (t) at the current moment is determined by the input x (t) at the current moment and the hidden state h (t-1) at the upper level. In addition, the RNN neurons share the weight parameter matrix at each time step.

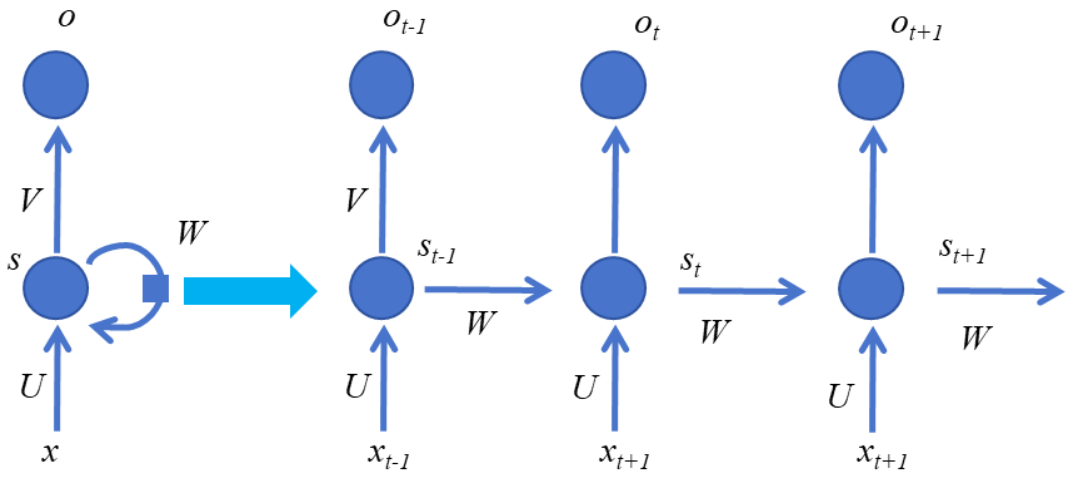

Fig. 3 Workflow of the RNN structure

As shown in Fig 3, when the neural network receives the measured value of interest x_t at time t, the value of the hidden layer is obtained by multiplying X_t with the default weight U, the value of the hidden layer is S_t, the O_t of the output value, and the key point is that the value of St depends not only on X_t but also on S_{t-1}. Four inputs of the AI machine -instantaneous surge displacement, velocity, pitch displacement, velocity - are provided by the physical model in the basin. These four parameters are initially model-scale but are simultaneously converted to full-scale by the Froude Scaling Law in the controller. The time history of the wind velocity

is pre-stored in the controller as the fifth input of the prediction module. The output is rotor thrust (which is the most significant aerodynamic impact for experimental research of OFWTs).

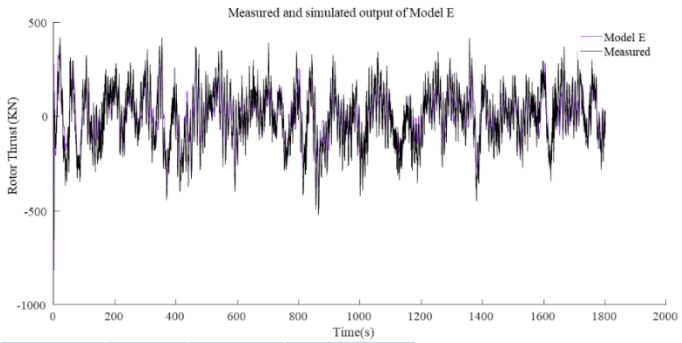

Case No.	Database Name	Size	Module	Accuracy	FPE	MSE
1	20Hz_80Hz_20Hz_20Hz	72000 *5	A	94.29%	65.38	65.32
2	20Hz_80Hz_20Hz_80Hz	36000 *5	B	94.4%	66.78	66.68
3	20Hz_80Hz_20Hz_20Hz	36000 *5	C	94.4%	66.78	66.68
4	80Hz_80Hz_80Hz_80Hz	144000 *5	D	96.41%	26.94	26.93
5	80Hz_80Hz_80Hz_20Hz	144000 *5	E	96.41%	26.94	26.93
6	80Hz_80Hz_20Hz_80Hz	36000 *5	F	92.04%	132.6	132.6
7	80Hz_80Hz_20Hz_20Hz	36000 *5	G	92.04%	132.6	132.6

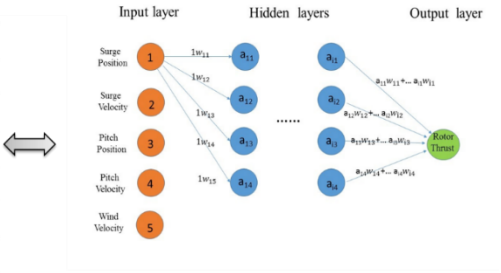

Fig. 4 The process of achieving the prediction module

As learnt from Fig. 4, 7 datasets are compared to secure the best model to be used in the AIReaTHM application. For example, when five simulated inputs are given to Model E, the predicted thrusts are gained and used to compare with the rotor thrust from FAST computation of the same inputs. Furthermore, seven trained models are compared in terms of final prediction error (FPE), and mean-square error (MSE), respectively. It is obvious that model D or model E should be used in the prediction module because they give the best prediction accuracy, while least prediction errors. The simulated output-rotor thrust obtained from prediction model E are comparatively given in Fig. 5. When selecting the datasets, four frequencies are considered, which are the frequency of the wind data(f1), the frequency of FAST calculation(f2), and the subsampling frequency of the data from the FAST calculation(f3), the frequency of training the prediction module(f4). The dataset is then named in ‘‘f1_f2_f3_f4’’. For each dataset, five vectors represent five individual parameters, which are pitch, pitch velocity, surge, surge velocity, and wind velocity, respectively.

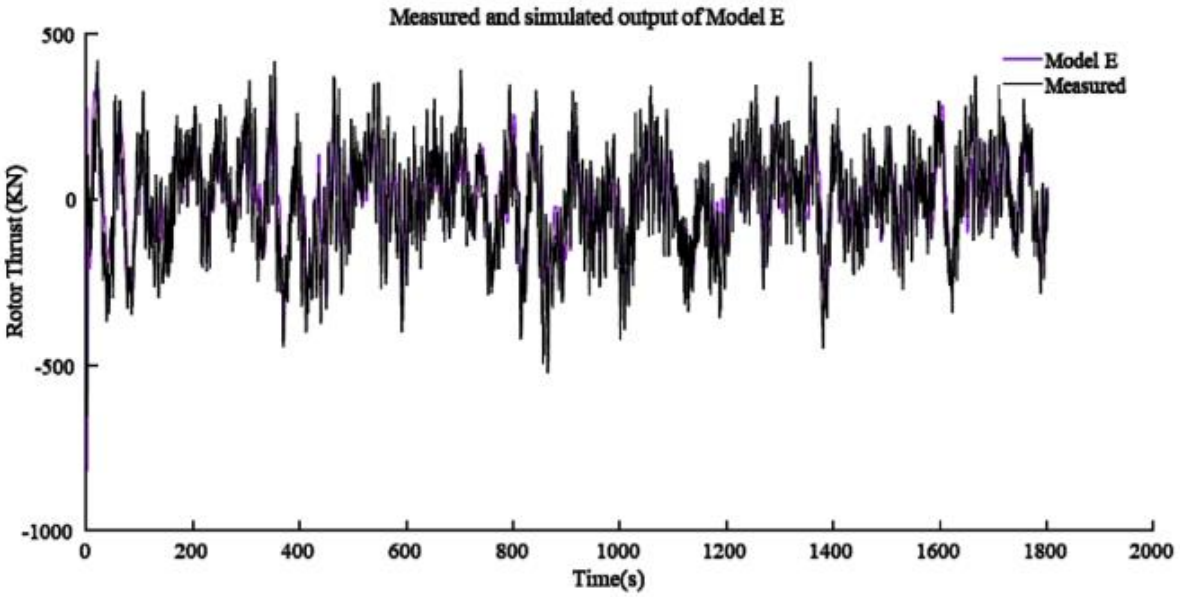

Fig. 5 The output of the prediction modules compared with the measured

Table 1 Optimization of the prediction model by using different datasets

Case No.	Database Name f1_f2_f3_f4	Database Size	Prediction model	Accuracy	FPE	MSE
1	20Hz_80Hz_20Hz_20Hz(+)	72000×5	A	94.29%	65.38	65.32
2	20Hz_80Hz_20Hz_80Hz	36000×5	B	94.4%	66.78	66.68
3	20Hz_80Hz_20Hz_20Hz	36000×5	C	94.4%	66.78	66.68
4	80Hz_80Hz_80Hz_80Hz	144000×5	D	96.41%	26.94	26.93
5	80Hz_80Hz_80Hz_20Hz	144000×5	E	96.41%	26.94	26.93
6	80Hz_80Hz_20Hz_80Hz	36000×5	F	92.04%	132.6	132.6
7	80Hz_80Hz_20Hz_20Hz	36000×5	G	92.04%	132.6	132.6

Regarding the database's data size, initial trials were conducted by extending the simulation time, resulting in an increased data size. Typically, as the simulation time increases, so does the prediction accuracy. However, there is a point at which further increasing the simulation time does not enhance the prediction accuracy, as observed in the comparison between case 1 and case 3. Therefore, the time boundary for running simulations was determined to be 2000s for case 2 to case 7, providing crucial insights for optimization analysis.

Table 1 demonstrates that the frequency of FAST computations (f3) significantly impacts the dataset size. Increasing f3 leads to a substantial growth in data size. As a result, Model D and Model E are trained using four times the data volume compared to Model B and Model C. It is evident that Model D and Model E exhibit superior prediction accuracy with fewer errors. The prediction accuracy of the targeted model is influenced not only by f3 but also by f1, as observed in the comparison between cases 2 & 3 and cases 6 & 7, in conjunction with case 2 and case 4, which helps draw conclusions. Additionally, it is clear that higher accuracy consistently corresponds to lower final prediction errors.

3 Construction of the AI-prediction-in-the-loop testing platform

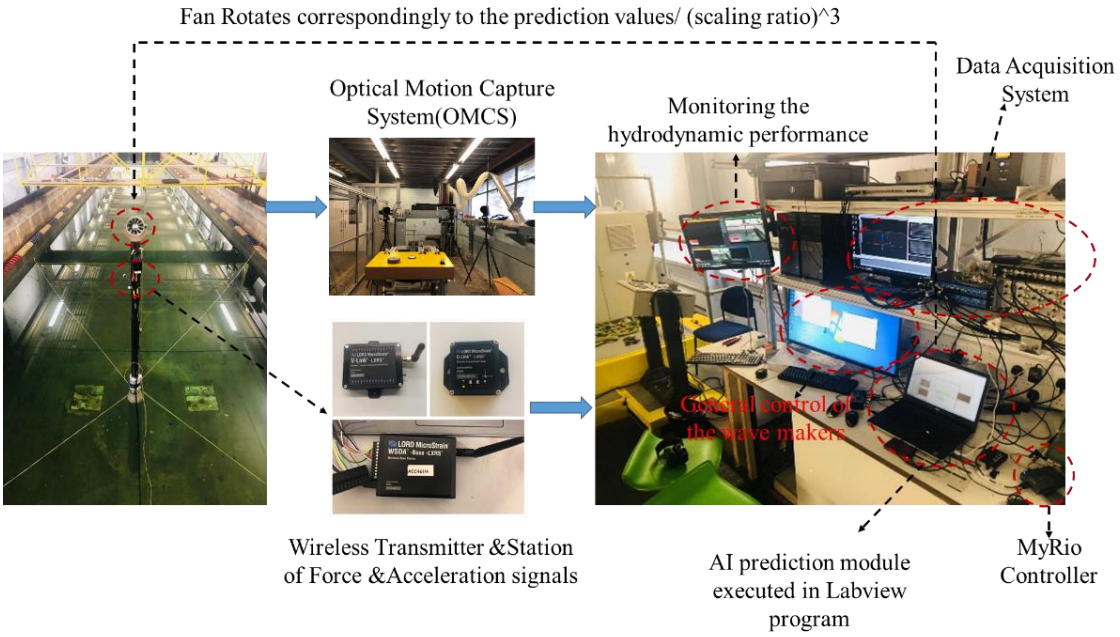

Fig. 6 Construction of the AIReaTHM testing platform

In the experimental loop of the AIReaTHM testing rig, as shown in Figure 6, the following key steps are involved: 1) An optical motion capture system measures surge and pitch motion parameters, including displacements and velocities, from the physical model placed in the water tank. 2)These motion parameters, along with pre-stored wind data in the computer random access memory (RAM), are transmitted to the prediction module via the data acquisition system (DAQ) system. 3)The prediction module generates the rotor thrust command, which drives the rotation of the fan and influences the motion response of the physical model.

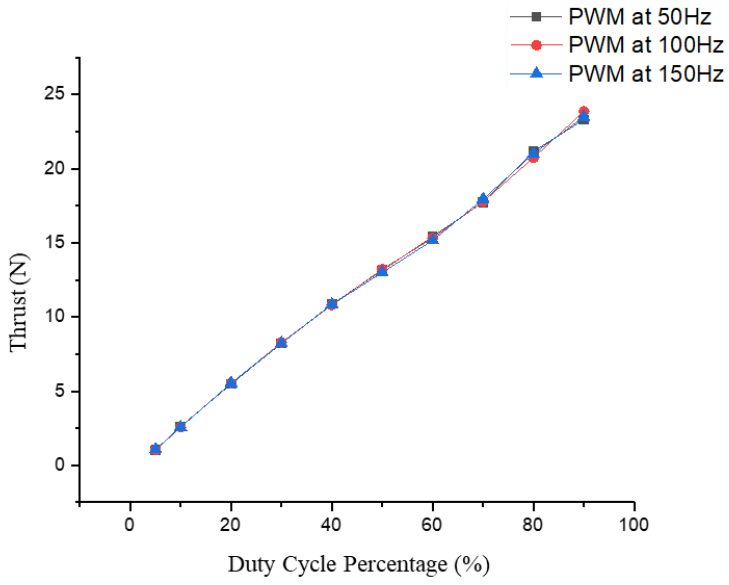

Fig. 7 The fan thrust of the calibration tests at different operating frequencies

Figure 7 displays the results of the calibration tests conducted on the fan, which involved controlling it at different operating frequencies. Prior to each benchmark test, the fan underwent calibration using a pulse width modulation (PWM) DC generator for speed control, ensuring precise measurements and reliable execution. The calibration test explored three frequencies (50Hz, 100Hz, and 150Hz) in order to identify the optimal operating frequency. However, as depicted in Fig. 7, the targeted rotor thrust was found to be largely unaffected by the operating frequency. Consequently, a frequency of 100Hz was chosen for the benchmark testing sessions. Furthermore, the calibration results indicated a strict and consistent linear correlation between the commanded thrust and the measured thrust of the fan. This linear relationship was subsequently employed to control the fan and attain the desired rotor thrust. Similarly, the load cell used in the experiment was also calibrated. By analyzing the sample points, a clear link between the thrust reading and voltage change of the load cell was discovered. To ensure accurate readings from the load cell, a regression analysis was conducted, resulting in the derivation of a regression equation, as illustrated in Figure 8.

a b

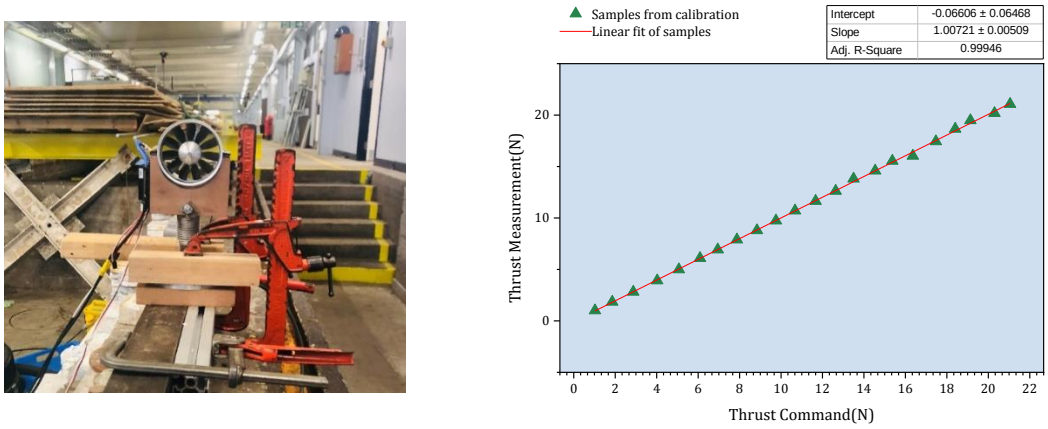

Fig. 8 Calibration of the executing fan

a b

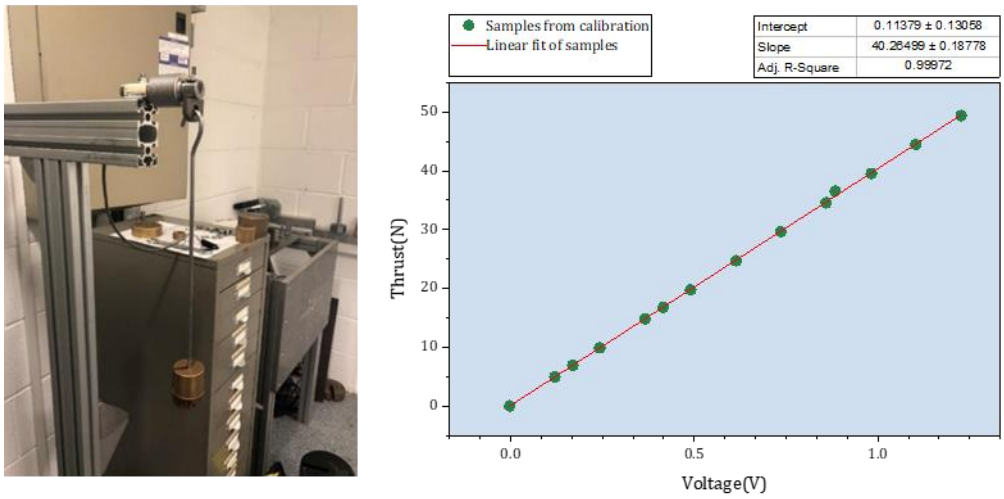

Fig 9 Calibration of the load cell

During the entire process, the controller effectively manages the scale interface considerations in the following way:

a) The inputs gathered at the model scale are converted to the full scale using the Froude Scaling Law within the controller. This conversion takes place before transferring the inputs to the prediction module.

b) As part of its output, the controller generates a command for the full-scale rotor thruster. In summary, the controller handles scale interface issues by utilizing the Froude Scaling Law to convert inputs from the model scale to the full scale. The controller then generates a command for the full-scale rotor thruster.

4 Benchmark testing arrangements

Benchmark tests are necessary to objectively evaluate the performance of the AI prediction, the ensure the feasibility of the AI-in-the-loop hybrid testing methodology, compare the testing effects with existing choices, and future-proof systems or components. They are vital tools for making informed decisions and optimizing technology for optimal performance and efficiency.

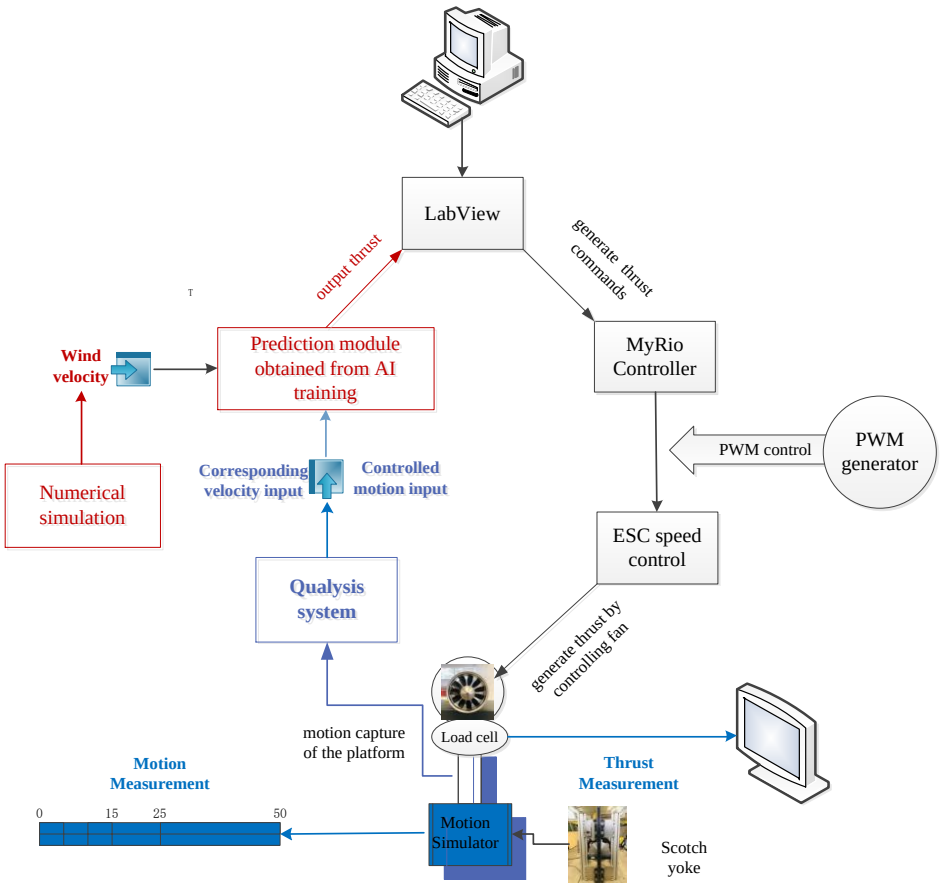

Fig. 10 Experimental set-up for benchmark testing

In order to assess the efficacy of the proposed AIReaTHM testing methodology, a benchmark testing platform (depicted in Fig.10) has been developed to investigate the accuracy of predicting and executing targeted real-time rotor thrust in an experimental setting. To simulate the surge input, a Scotch Yoke mechanism is employed, and the rotor thrust signal is

monitored by the DAQ system. While the surface waves and ocean currents are physically modelled in the tank using wake makers, the turbulent wind is generated numerically and pre-stored in the controller as oncoming wind input for the prediction module. The thrust calculation is carried out in full scale in the prediction module, and the red lines in Fig. 10 indicate the numerical and software parts of the hybrid testing approach, while the blue lines represent the physical substructures. The hardware used to execute the thrust command is illustrated by grey cubes and circles. A controller is utilized to read the motion and velocity profiles of the motion simulator, and they are scaled up to full scale using the Froude scaling law before being entered into the prediction module in the controller, along with the full-scale wind field data produced via numerical simulation. Subsequently, the software in the controller computes the corresponding thrust. To accommodate model-scale experiments, the profile of the real-time thrust command is scaled down to model scale to drive the fan and generate fan thrust. A series of bench tests are carried out in this manner. In the benchmarking testing methodology, two measurements have been incorporated. Firstly, the Linear Variable Differential Transformer (LVDT) is utilized to accurately quantify the motion generated by the Scotch Yoke mechanism, enabling a comprehensive assessment of the motion capture quality of the Qualysis motion capture system. Additionally, a load cell is strategically positioned beneath the fan to precisely measure the total horizontal force exerted during its linear surge along the Scotch Yoke mechanism.

For the AI predicting model, two modes are currently enabled: mode A and mode B. The prediction algorithm for mode A is specifically employed for regular wave conditions (with frequencies ranging from 0.1 rad/s to 3.0 rad/s) and steady wind conditions (with wind speeds ranging from 6 m/s to 18 m/s). On the other hand, the prediction algorithm for mode B is developed to forecast outcomes in five distinctive sea states, characterized by wave spectrum and the IECKAI turbulent wind model. To empirically validate the performance of both algorithms, a comprehensive set of benchmark tests has been meticulously designed and outlined in Table 2.

Table 2 Testing arrangement

Mode	**Quantity of tests**	**Wind**	**Wave condition**	**surge**
A	5	8m/s	Regular wave(f= 0.1rad/s, 0.2 rad/s, …3.0rad/s)	Surge at five frequency(v1,v2,v3,v4,v5)
A	5	10m/s		
A	5	12m/s		
A	5	14m/s		
A	5	16m/s		
Mode	Quantity of tests	Sea State		surge
B	5	SS1	SS1+	Surge at five frequency(v1,v2,v3)
B	5	SS2	SS2+	
B	5	SS3	SS3+	
B	5	SS4	SS4+	
B	5	SS5	SS5+	

v1…v5 is used to present the five surge frequencies to differ from f1…f4 in section 2.2

5 Outcomes of the benchmark testing and necessary data process

To accurately measure the rotor thrust generated by the fan, a load cell is integrated beneath the fan. It is worth mentioning that the load cell is securely attached to the Scotch Yoke

mechanism and moves in sync with the fan during operation. Consequently, the reading obtained from the load cell consists of two significant components: 1) the acceleration force, and 2) the rotor thrust on a model scale, which will be referred to as "thrust" for simplicity in this paper. Hence, it is crucial to eliminate the contribution of the acceleration force from the load cell's reading.

Determining the appropriate mass to eliminate the real-time acceleration force from the load cell's measurement time histories is crucial. To achieve this, the referred mass is calculated, statistically analyzed, and cross-verified with the masses of both the physical fan and its holder. Once the acceleration force has been successfully eliminated from the load cell's experimental readings, the measurement of the fan's thrust can be obtained. To identify the referred mass, a series of experiments were conducted where only surge motions were allowed while the fan rotation was switched off. In this case, the load cell's readings solely captured the acceleration force. Figure 11 illustrates the readings from a typical experiment, where velocity is derived by differentiating the LVDT (Note: LVDT refers to Linear Variable Differential Transformer, which is a type of sensor used for measuring displacement or position) reading, and acceleration(a) is obtained by further differentiating the velocity.

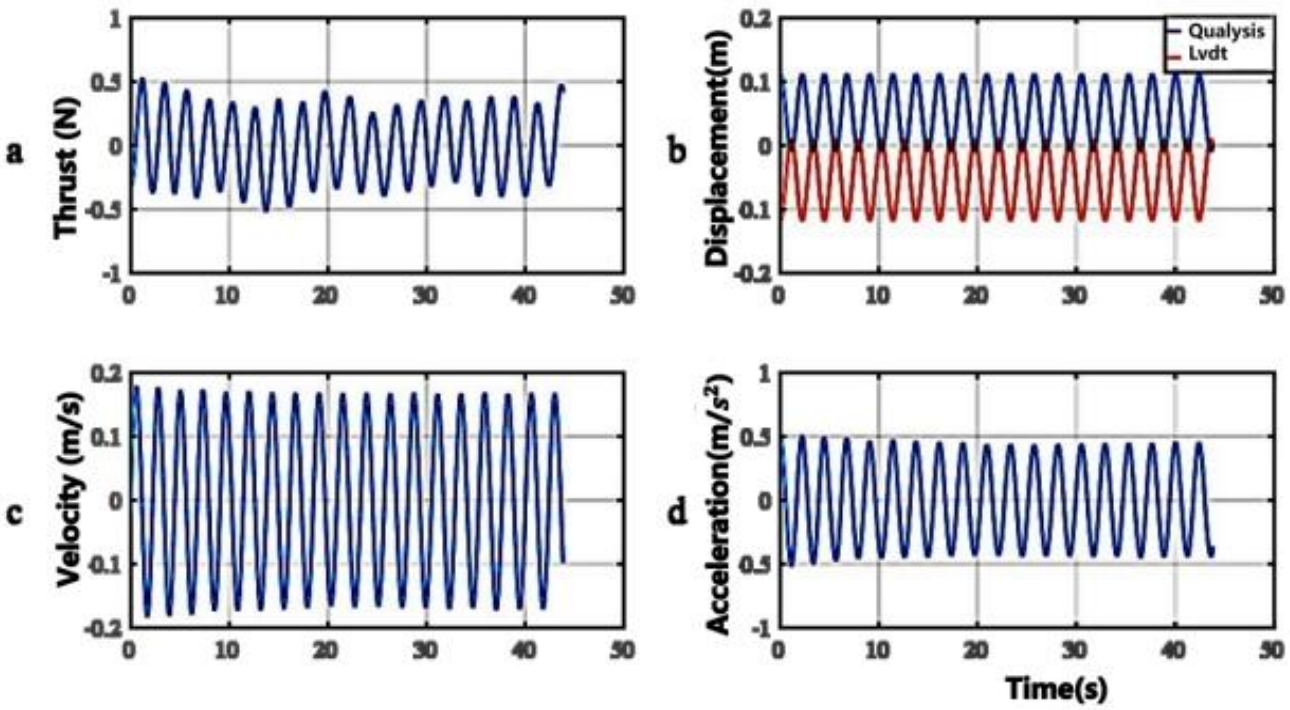

Fig. 11 A typical experiment without fan rotating

The acceleration force can be described as Eq(2) by Newton's Second Law

$$F_{referred} = M_{referred} \times a \tag{1}$$

then, $F_{referred}$ and acceleration a are following

$$F_{referred} = |F_{\max}| \sin(wt + \varphi_1) \tag{2}$$

$$a = |a_{\max}| \sin(wt + \varphi_2) \tag{3}$$

where, w is the angular frequency of the motion simulator (Scotch Yoke). If we ignore the phase difference, the mass causes the initial force can be described as,

$$M_{referred} = |F_{\max}| \div |a_{\max}| \quad (4)$$

then the distribution of the referred mass obtained by the above experiment varies as $|F_{\max}|$ and $|a_{\max}|$ vary per cycle, which is demonstrated in in Fig. 12(a). In the same manner, the referred mass is calculated on a per-cycle basis, afterwards, the mean value as well as the variance are obtained for each test as shown in Fig. 12(b). Based on the statistical calculation of the experiment data, it is recommended that the range of the referred mass located between 820-830g.

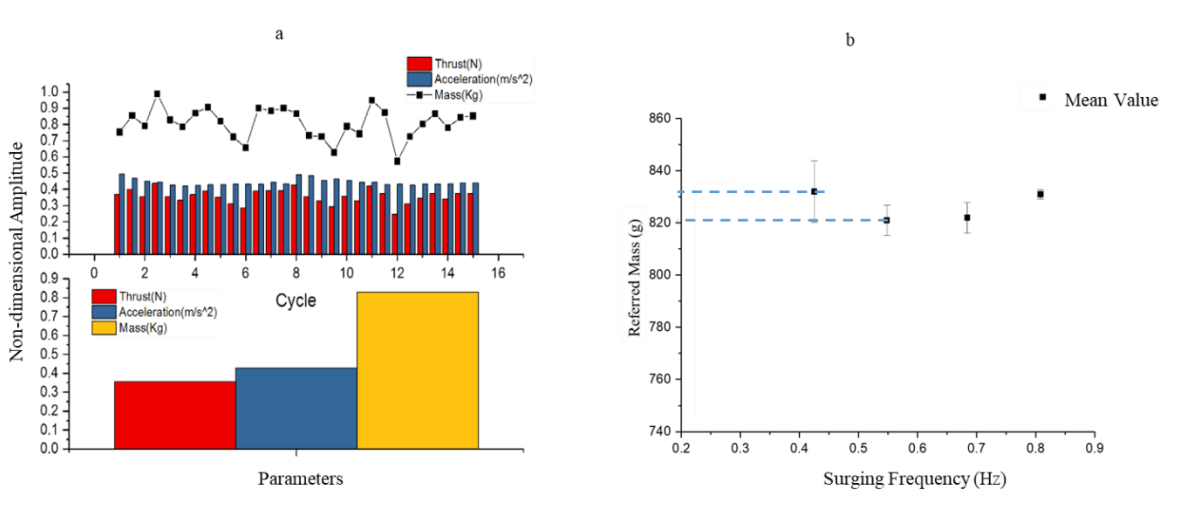

Fig. 12 Distribution of the initial mass in one typical experiment

To eliminate the acceleration force from the load cell's experimental readings, it is necessary to determine the appropriate referred mass. The referred mass should be a constant value that includes both the physical fan and load cell. However, since the load cell is only partly located above the surging piston, its 1/4 mass needs to be added to the mass of the fan for an accurate measurement. To determine the referred mass, the mass of the relevant parts was measured. According to Fig. 13, the mass of the fan was determined to be 718g, while the 1/4 mass of the load cell was calculated as 102g. The total referred mass was calculated as 820g, which is within the recommended range. This value was used to remove the acceleration force from the load cell's readings. The remaining portion of the load cell's readings provides a reference to analyze the fan's ability to generate a commanded thrust, which is useful when validating the AIReaTHM testing methodology. This referred measurement is denoted as RM.

Fig. 13 Weight of the mass of the physical fan and load cell

This measurement of fan thrust serves various purposes within the study. Firstly, it aims to validate the practicality of the AIReaTHM testing methodology. Secondly, it aims to explore the influence of surging motion on predicted rotor thrust. Thirdly, it aims to investigate the impact of turbulence and wave spectrum on rotor thrust. Lastly, it aims to identify the systematic uncertainties of the temporary testing rig used for validating the testing methodology. By doing so, it paves the way for further enhancement and refinement of the testing methodology.

6 Validation of the AIReaTHM testing platform

6.1 The comparative analysis between the measured and AI-predicted rotor thrust

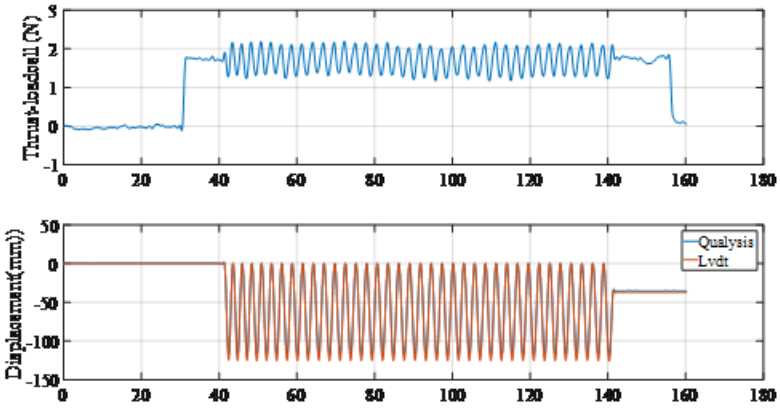

Fig. 14 Measurement from one typical bench test

Figure 14 displays data from a typical experiment where wind speed is 12 m/s, and the motion simulator surges at v2. The data between 60 and 130 seconds is selected for analysis to eliminate transient reactions. Initially, the load cell reading is adjusted by removing the acceleration force to obtain RF. Subsequently, the remaining data is scaled by the Froude scaling law. In Figure 15, a comparison is presented between the AI command and the scaled-up values of the generated fan thrust, when wind speed is set to 8 m/s, 10 m/s, 12 m/s, 14 m/s, and 16 m/s. The measurements agree well with the AI prediction output when the wind speed is 8 m/s, 12 m/s, and 16 m/s. However, for a wind speed of 10 m/s and 14 m/s, there are some amplitude errors, which can be attributed to the randomness of the real-time fan thrust

measurement. As the fan rotates, various random factors may affect the thrust measurement, such as ground vibrations from pedestrians, air flows caused by opening or closing doors, and environmental noise resulting from the operation of other testing equipment in the lab. Thus, it can be concluded that the fan can function adequately as per the AI signal commands. Also, both the AI values and the scaled-up FM values concur with the conclusions presented in [4], namely, that the average rotor thrust corresponds to the low-frequency component of the rotor thrust, which is primarily driven by wind speed. On the other hand, the oscillating component of the rotor thrust corresponds to its high-frequency component, which is mainly driven by wave conditions.

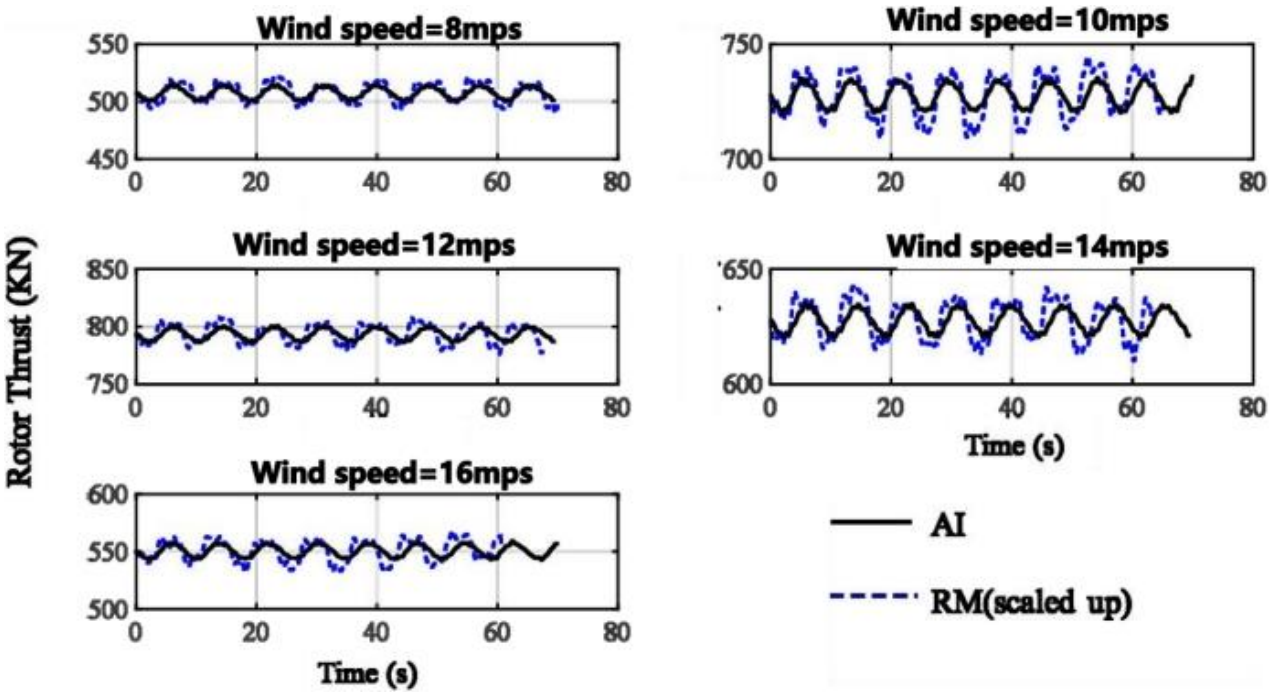

Fig. 15 RM compared with AI rotor thrust, surge at v1, various wind speeds

6.2 The effect of surge frequency and wind speed on the rotor thrust

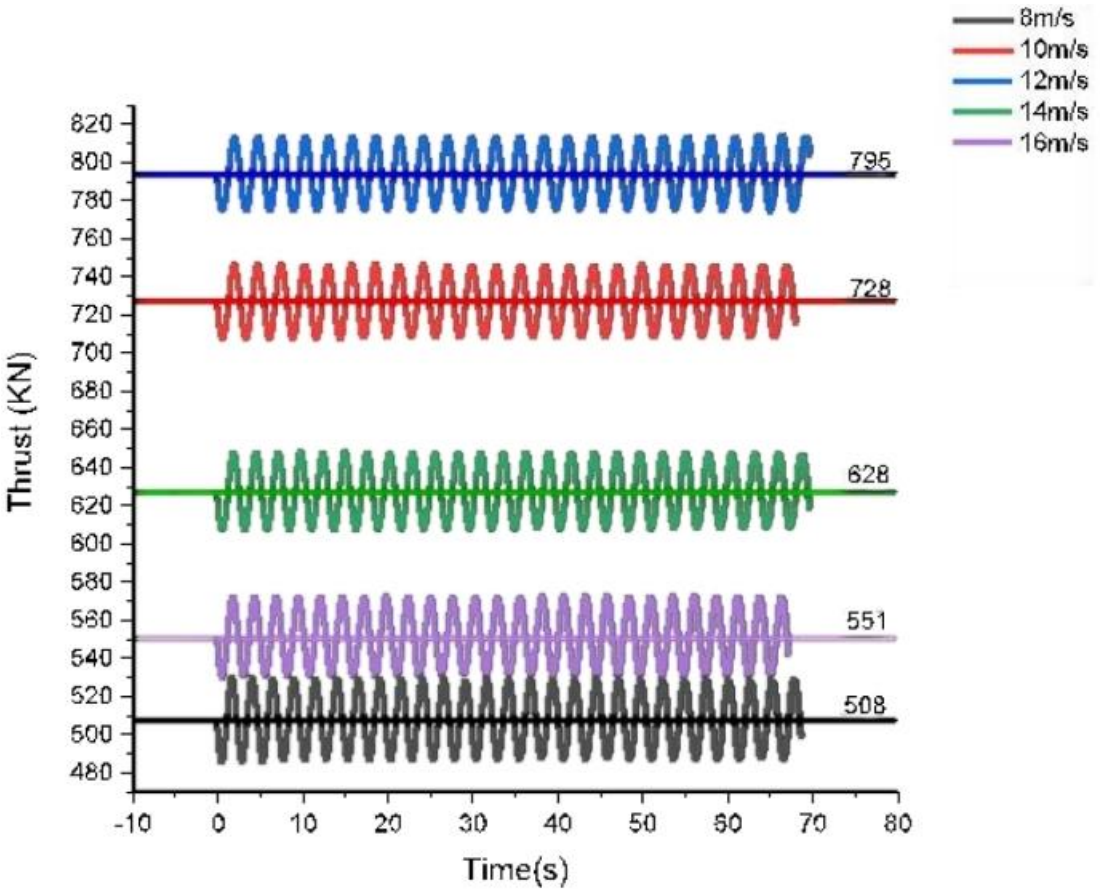

Fig. 16 Same surge frequency under different wind speeds

To gain more comprehensive insights into the performance of the prediction module, we conducted a case study on surging at v2. As shown in Figure 16, we compared the thrusts obtained under various wind speeds, which revealed differences in their average values. However, the oscillating component of the thrusts exhibited similar responses, which is reasonable since the surge inputs remained the same. Moreover, our bench test results suggest that the surge input did not impact the average value of the thrusts. In Figure 17, we examined the thrusts produced under the same wind speed, but with the motion simulator surging at different frequencies. Our findings showed that increasing the frequency of the surge input led to a corresponding increase in the frequency of the oscillating component of the thrust. Furthermore, the amplitude of the oscillating component increased slightly as the frequency rose.

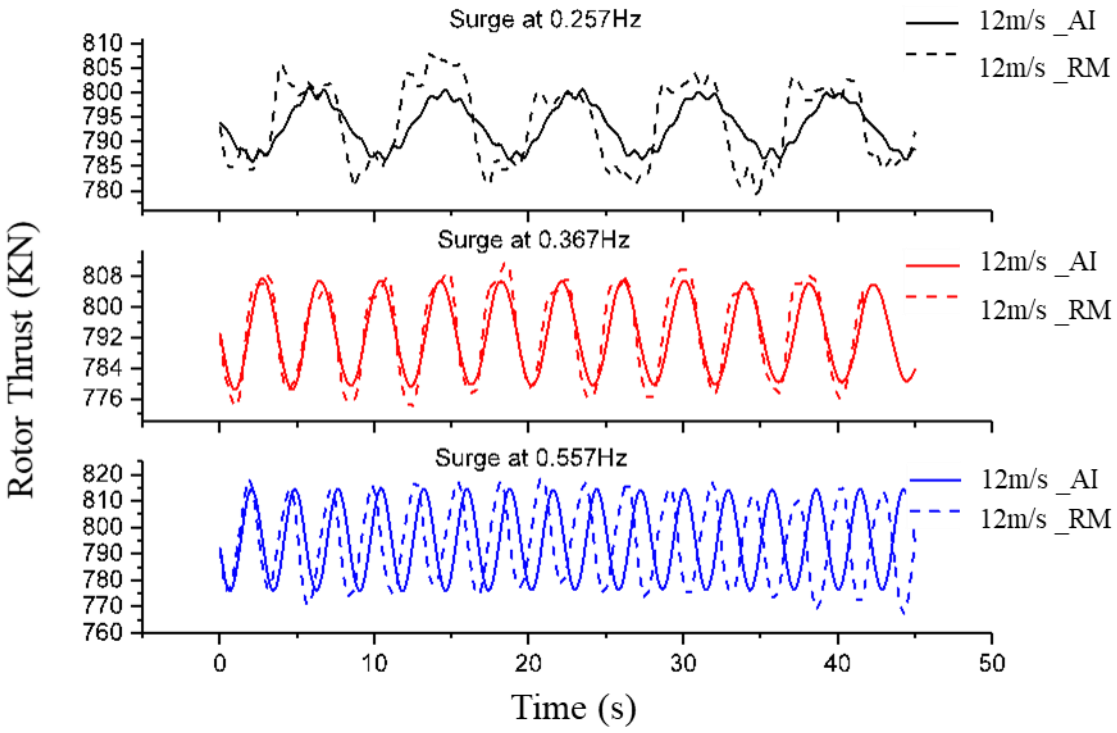

Fig. 17 Same wind speed under different surge frequencies

Our analysis revealed a minor frequency difference between the AI command and the measured rotor thrust (RM), as illustrated in Fig. 17. At the highest surging speed, corresponding to a frequency of 0.557Hz, this frequency difference became more noticeable. We also found that the frequency of the oscillating component of the thrust increased as the frequency of the surge input rose. Additionally, the amplitude of the oscillating component slightly increased with frequency. This is likely caused by the simplifying assumption we made when abstracting the measurement of rotor thrust from the load cell reading. The calculation of the acceleration force is sensitive to acceleration, which is derived from the surge motion. Moreover, the RM is an external reference rather than an absolute standard and is not part of the testing methodology. Therefore, the RM values do not affect the performance of the AI prediction module. To exercise caution in our experimental research, any frequency/time difference issues were studied further on a case-by-case basis in "Development and characterisation of an AI-in-the-loop testing platform for floating wind turbines part II: benchmark tests, uncertainty discussion, and comparative studies".

6.3 The effect of turbulence and wave spectrum on the rotor thrust

Table 3 provides a breakdown of the wave and wind conditions for each sea state. The JONSWAP spectrum with varying parameters is employed to represent the wave conditions. In terms of wind conditions, we utilize five IECKAI models with turbulence for SS1-SS2 (referred to as 'SSi' together as needed thereafter) and SS1+ to SS5+ (together referred to as 'SSi+' as needed thereafter) to compare against the corresponding steady wind of each SSi. The parameters of JONSWAP spectrum in Table 3 are defined according to Eq. (7).

$$S(\omega)=\frac{\alpha g^2}{\omega^5}\exp\{-1.25\left(\frac{\omega_p}{\omega}\right)^4\}\gamma^{\exp(-0.5(\frac{\omega-\omega_p}{\sigma\omega_p})^2)} \quad (5)$$

where $\alpha=5.061\left(\frac{\omega_p}{2\pi}\right)^4 H_s^2[1-0.287\log\gamma]$; $\sigma=0.07$ for $\omega<\omega_p$, and $\sigma=0.09$ for $\omega\geq\omega_p$; $\omega_p=2\pi/T_p$. H_s is the significant wave frequency, T_p is the peak wave period, γ is the peak enhance coefficient.

Table 3 Environmental conditions of sea states

Sea State	Wave Conditions(JONSWAP spectrum)	Wind Conditions(IECKAI model)
SS1	H_s =4.55 m, T_p =9.00s, γ =2.45	$\bar{u}$ =11.40, TI=20.45
SS2	H_s =1.5 m, T_p =6.61s, γ =1	$\bar{u}$ =11.40, TI=20.45
SS3	H_s =1.25 m, T_p =6.36s, γ =1	$\bar{u}$ =9.18, TI=22.98
SS4	H_s =1.75 m, T_p =6.86s, γ =1	$\bar{u}$ =12.8, TI=19.31
SS5	H_s =2.75 m, T_p =7.8s, γ =1.41	$\bar{u}$ =16.8, TI=17.09
SS1+	H_s =4.55 m, T_p =9.00s, γ =2.45	$\bar{u}$ =11.40, TI=0
SS2+	H_s =1.5 m, T_p =6.61s, γ =1	$\bar{u}$ =11.40, TI=0
SS3+	H_s =1.25 m, T_p =6.36s, γ =1	$\bar{u}$ =9.18, TI=0
SS4+	H_s =1.75 m, T_p =6.86s, γ =1	$\bar{u}$ =12.8, TI=0
SS5+	H_s =2.75 m, T_p =7.8s, γ =1.41	$\bar{u}$ =16.8, TI=0

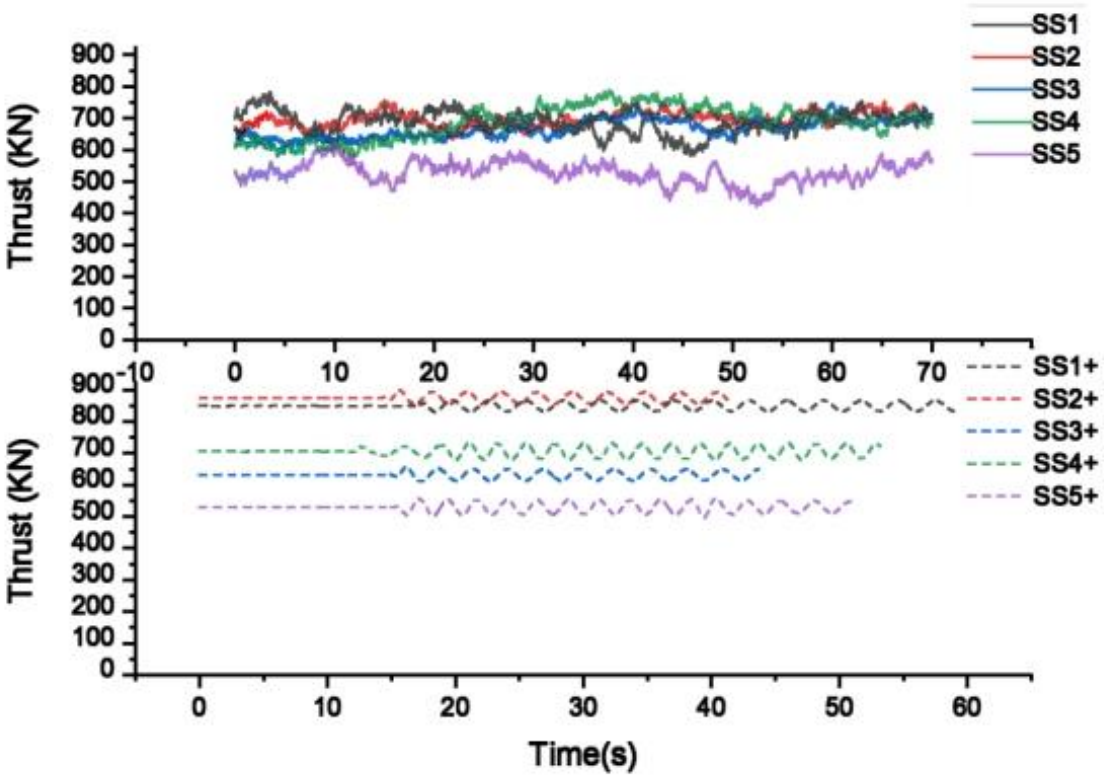

Fig. 18 Time histories of rotor thrusts under different sea states

After conducting benchmark tests for the sea states outlined in Table 3, thrust samples were obtained during motion simulation at v2 for ten different sea states, as shown in Fig. 18. This figure provides valuable insights in several ways. Firstly, unlike other sea states with steady wind conditions such as SSi+, the thrust obtained for sea states with turbulent wind tends to be erratic and random, demonstrating the impact of turbulence on rotor thrust. Notably, the mean thrust of SS1 appears to decrease slightly compared to SS1+, with similar drops observed in SS2 to SS5, indicating that turbulence affects both instantaneous and mean thrust. While wind conditions are identical for SS1 and SS2, different wave parameters are used to generate waves in the basin, causing their split-second thrust to follow different trajectories. However, the mean thrust remains almost the same, suggesting the wave conditions have minimal influence on rotor thrust. The mean thrust initially increases as wind speed rises, but once it reaches its peak at 12m/s, it begins to decline slowly, reaffirming that wind speed remains the most significant factor affecting rotor thrust, though turbulence also plays a role. While the impact of the wave spectrum on rotor thrust is evident, it is minimal compared to the effect of wind conditions.

Furthermore, in the experiments conducted on SS1 and SS2, the wind conditions were kept constant, but different wave parameters were used to generate waves in the testing basin. This resulted in different trajectories for the split-second thrust of SS1 and SS2, while the average thrust remained relatively stable. These findings suggest that wave conditions may have only a minor impact on rotor thrust. Notably, the average thrust initially increases with wind speed, reaching its peak at 12m/s before gradually declining. This indicates that wind speed remains the primary factor affecting rotor thrust, although turbulence also plays a role.

While the wave spectrum does contribute to rotor thrust, its effect is relatively insignificant compared to that of wind conditions.

The originality of applying artificial intelligence techniques in the hybrid testing method for floating wind turbines can be summarized as follows: Firstly, this experimental method addresses the issue of the Froude-Reynold scaling conflict in hybrid model testing by enabling full-scale prediction calculations of aerodynamic loads. Secondly, it replaces numerical simulation with AI prediction to improve the calculation speed of rotor thrust and reduce the delay effect of hybrid model experiments. Lastly, the AI prediction machine used in this method does not rely on any third-party computing software. It can be continuously optimized and upgraded with the accumulation of experimental data and prototype operation data, significantly enhancing the accuracy of floating wind turbine model testing while reducing the cost of experimentation.

7 Conclusions and future work

We have proposed and constructed a novel AI-based hybrid testing rig, which has been subjected to benchmark tests using a manoeuvrable motion simulator. The study investigates the impact of surge inputs (generated via motion simulation), wind speeds, and turbulence wind on targeted thrust. The research has yielded several significant new contributions, including:

- The benchmark testing results demonstrate that the AI-in-the-loop testing methodology can overcome the Froude-Renald scaling conflict in the tank testing of floating wind turbines.
- Turbulence wind significantly influences the amplitude of motions.
- Waves have less influence on the hydrodynamic response of the floating spar than turbulence wind.
- The frequency of motions has a significant impact on the time delay between the prediction and measurement of rotor thrust.

Moreover, it should be noted that the AI machine relies on big data from the cloud to train its prediction algorithms. As more realistic data become available from pilot floating wind farms, the AI machine's performance will improve.

Acknowledgements

The authors acknowledge the financial support provided by the National Key R&D Program of China (No. 2022YFE0207000), National Natural Science Foundation of China (No. 52101329) and National Engineering Research Center for Offshore Windpower (NoHSFD22004).

Reference

1. Wind Europe. *Floating Offshore Wind Vision Statement*. 2017. https://windeurope.org/wp-content/uploads/files/about-wind/reports/Floating-offshore-statement.pdf

2. EUROPEAN COMMISSION. *REPowerEU: Joint European Action for more affordable, secure and sustainable energy*. Strasbourg, 2022. https://energy.ec.europa.eu/system/files/2022-03/REPowerEU_Communication_with_Annexes_EN.pdf

3. Department for Business, Energy & Industrial Strategy, Department for Energy Security & Net Zero, Prime Minister's Office. *British energy security strategy.* Updated 7 April 2022. https://www.gov.uk/government/publications/british-energy-security-strategy/british-energy-security-strategy

4. Mette, F., et al. *THE ESBJERG DECLARATION on The North Sea as a Green Power Plant of Europe*. 2022. https://news.belgium.be/sites/default/files/news-items/attachments/2022-05/The%20Esbjerg%20Declaration%5B99%5D.pdf

5. Goupee, A.J., et al. *Experimental comparison of three floating wind turbine concepts*. Journal of Offshore Mechanics and Arctic Engineering, 2014.**136**: 021903.

6. Vilsen, S.A., et al. *Method for Real-Time Hybrid Model Testing of ocean structures: Case study on horizontal mooring systems.* Ocean Engineering, 2019. **172**: p. 46-58.

7. Network, M.R.I. *Report on physical modelling methods for floating wind turbines*. MARINET report, 2015.

8. Day, A.H., et al., *Realistic simulation of aerodynamic loading for model testing of floating wind turbines*. 2017.

9. Bayati, I., et al. *6-DoF hydrodynamic modelling for wind tunnel hybrid/HIL tests of FOWT: the real-time challenge*. in *ASME 2018 37th International Conference on Ocean, Offshore and Arctic Engineering*. 2018. American Society of Mechanical Engineers Digital Collection.

10. Azcona, J., et al. *Aerodynamic thrust modelling in wave tank tests of offshore floating wind turbines using a ducted fan*. in *Journal of Physics: Conference Series*. 2014. IOP Publishing.

11. Giahi, M.H., et al. *Investigating the influence of dimensional scaling on aerodynamic characteristics of wind turbine using CFD simulation*. Renewable Energy, 2016. **97**: 162-168.

12. Make, M., Vaz, G. *Analyzing scaling effects on offshore wind turbines using CFD*. Renewable Energy, 2015. **83**: 1326-1340.

13. Make, M.K.P. *Predicting scale effects on floating offshore wind turbines: A numerical analysis of model- and fullscale wind turbines using a RANS CFD solver*, 2014. TU Delft, Delft, The Netherlands.

14. Bayati, I., Belloli, M., Bernini, L., et al. *Aerodynamic design methodology for wind tunnel tests of wind turbine rotors*. Journal of Wind Engineering and Industrial Aerodynamics, 2017. **167**: 217-227.

15. Martin, H.R., Kimball, R.W., Viselli, A.M., et al. *Methodology for wind/wave basin testing of floating offshore wind turbines*. Journal of Offshore Mechanics and Arctic Engineering, 2014. **136**: 2.

16.Bayati, I., et al., Design of a 6-DoF robotic platform for wind tunnel tests of floating wind turbines. Energy Procedia, 2014. 53: p. 313-323.

17.Bachynski, E.E., V. Chabaud, and T. Sauder, Real-time hybrid model testing of floating wind turbines: sensitivity to limited actuation. Energy Procedia, 2015. 80: p. 2-12.

18.Chabaud, V., et al., Multiple-degree-of-freedom actuation of rotor loads in model testing of floating wind turbines using cable-driven parallel robots. Journal of Physics: Conference Series, 2018. 1104: p. 012021.

19.Berthelsen, P.A., et al. Real-time hybrid model tests of a braceless semi-submersible wind turbine: Part III—Calibration of a numerical model. in ASME 2016 35th International Conference on Ocean, Offshore and Arctic Engineering. 2016. American Society of Mechanical Engineers Digital Collection.

20.Sauder, T., et al. Real-time hybrid model testing of a braceless semi-submersible wind turbine: Part I—The hybrid approach. in ASME 2016 35th International Conference on Ocean, Offshore and Arctic Engineering. 2016. American Society of Mechanical Engineers Digital Collection.

21.Bachynski, E.E., et al. Real-time hybrid model testing of a braceless semi-submersible wind turbine: Part II—Experimental results. in ASME 2016 35th International Conference on Ocean, Offshore and Arctic Engineering. 2016. American Society of Mechanical Engineers Digital Collection.

22.Cermelli, C., D. Roddier, and A. Aubault. WindFloat: a floating foundation for offshore wind turbines—part II: hydrodynamics analysis. in ASME 2009 28th International Conference on Ocean, Offshore and Arctic Engineering. 2009. American Society of Mechanical Engineers Digital Collection.

23.Jiang, X., et al., Analysis and real-time prediction of the full-scale thrust for floating wind turbine based on artificial intelligence. Ocean Engineering, 2019. 175: p. 207-216.

24.Jiang, X., S. Day, and D. Clelland, An innovative generic platform to simulate real-time PTO damping forces for ocean energy converters based on SIL method. Ocean Engineering, 2018. 170: p. 209-221.

25.Jiang, X., Software-in-the-loop applications for improved physical model tests of ocean renewable energy devices using artificial intelligence. 2020, University of Strathclyde.

26.Jiang, X., S. Day, and D. Clelland, Hydrodynamic responses and power efficiency analyses of an oscillating wave surge converter under different simulated PTO strategies. Ocean Engineering, 2018. 170: p. 286-297.